Micromotion-Enhanced Fast Entangling Gates For Trapped Ion Quantum Computing

Alexander K. Ratcliffe, Lachlan M. Oberg, and Joseph J. Hope
*Department of Quantum Science, RSPE, Australian National University**
(Dated: February 19, 2019)

RF-induced micromotion in trapped ion systems is typically minimised or circumvented to avoid off-resonant couplings for adiabatic processes such as multi-ion gate operations. Non-adiabatic entangling gates (so-called 'fast gates') do not require resolution of specific motional sidebands, but we find that gates designed for micromotion-free environments have significantly reduced fidelity in the presence of micromotion. We show that when fast gates are designed with the RF-induced micromotion in mind, they can in fact out-perform fast gates in the absence of micromotion. This enhancement is present for all trapping parameters and is robust to realistic sources of experimental error. This result paves the way for fast two-qubit entangling gates on scalable 2D architectures, where micromotion is necessarily present on at least one inter-ion axis.

Quantum computing offers the promise of boosting our current computational capabilities, outperforming certain known classical algorithms, and allowing tractable simulations of complex quantum systems [1]. To realise this potential, a quantum information processing (QIP) architecture must be able to scale to large numbers of qubits, providing the ability to perform quantum algorithms to solve problems which are currently intractable with classical algorithms. Many platforms have been proposed as QIP architectures including superconducting qubits [2], defect centres in diamonds [3], single photons [4], NMR [5], topological qubits [6], quantum dots [7], and spin-spin interactions in silicon donor sites [8]. Many of these platforms have made significant progress towards the requirements for scalable quantum computing [9–11], demonstrating the required single and two-qubit fidelities [12–15]. However, these have been limited either by scalability or the number of operations achievable before state decoherence. To date, trapped ions have been a frontrunner of QIP architectures, demonstrating the largest numbers of qubits used in an algorithm, entangled states beyond the ability to make full state tomography and numerous demonstrations of quantum algorithms [16–20].

The key limitation in all QIP platforms is the number of high fidelity two-qubit gate operations that can be achieved within the decoherence time of the qubit. Fault tolerant quantum computation requires that enough of these operations can be conducted with high enough fidelities to correct for both errors in the gate operations and state decoherence. For surface codes, these limits are modest and require fidelities higher than 98% [12]. Although numerous implementations of side-band resolving adiabatic gates have demonstrated sufficient fidelities [19, 21, 22], these gates are too slow to allow for classically unrealisable computation within the decoherence time of the system.

Fast gates using ultra-fast pulses are poised to resolve this situation [23–26]. These gate schemes use state-dependent kicks from ultra-fast π-pulses to the ions, inducing state-dependent motion. This then becomes a state-dependent phase shift mediated by the Coulomb
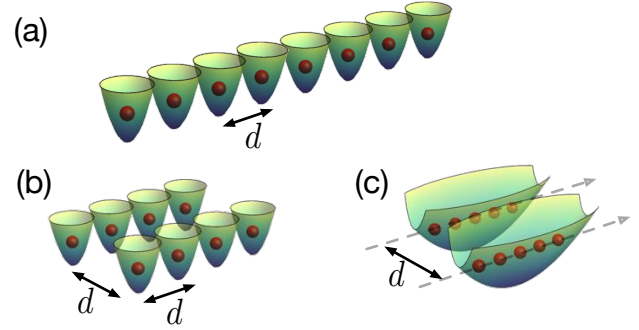

FIG. 1. (a) Diagram with a 1D lattice of trapped ions sitting in individual microtraps separated by a distance d. In this letter, we model this situation. In the future, more scalable arrangements will likely consist of arrays of traps holding single or multiple ions, as shown in parts (b) and (c). Fast gates can then be used efficiently between nearby ions from different traps, without need for the potentials to be changed, or for the ions to be moved.

interaction. A controlled phase gate will result when the laser pulses produce the correct phase shift and return the ions to their original motional state. Gate times are considerably shorter than adiabatic gates and high fidelities can be obtained. The feasibility of these schemes has been shown in recent experimental demonstrations [27–29]. So far, these schemes have only been applied to linear Paul traps in which the ions are arranged linearly in a common trap. This architecture is limited in its scalability. When the number of ions in the trap is increased, the longitudinal trapping frequency must be lowered to prevent buckling, which then slows both adiabatic and fast gates conducted on the longitudinal motional modes [25, 30]. However, fast gates can also operate between individual traps with a fidelity that asymptotes as the ion number increases [31]. Possible arrangements of these microtraps are linear or as 2D arrays, as depicted in Fig. 1 (a) & (b) respectively. Fast gates are also compatible with an architecture arranging adjacent linear Paul traps, as in Fig. 1 (c). In this architecture, gates between ions in adjacent traps can be conducted as they

would in a linear microtrap array and gates between ions in the same trap can be conducted as normal. A key difference between linear and multi-dimensional trap geometries is that the pulses used in the gate scheme cannot always stay transverse to the micromotion. Here we examine gates between ions in separate microtraps using their longitudinal motion and between ions in the same linear Paul trap using their axial modes.

Ion traps use an oscillating RF potential to generate a 3D trapping potential. The resulting dynamics approximate a simple harmonic oscillator, but with the addition of a rapid oscillation induced by the RF frequency, or micromotion [32]. Micromotion has thus far largely been treated as an undesirable effect, or has been ignored. Although micromotion is generally absent from the longitudinal axis of a linear Paul trap, it complicates the use of the axial mode which would otherwise provide the benefit of operating at a higher trapping frequency. Micromotion would also impact the operation of gates in 2D architectures such as microtraps or Wigner crystals formed in Penning traps [33, 34]. Recently it has been shown that when micromotion has been properly accounted for, it does not inhibit the ability to apply high fidelity entangling operations for sideband-resolving geometric phase gates using a continuously shaped laser pulse [35].

In this work, we show that micromotion can be used to enhance specifically designed fast gates using ultrafast pulses by orders of magnitude in fidelity for some experimentally accessible parameter regimes. This improvement is present both in the axial modes of a linear Paul trap and in a microtrap system, and exists for all trap parameters. We also show that these gates are robust to realistic sources of experimental error. We propose a novel technique to make use of this enhancement without significant alteration of current experimental set-ups.

We used gate schemes which are a generalisation of the Fast Robust Anti-symmetric Gate (FRAG) scheme [36], a variant of the GZC scheme [37]. They consist of six groups of counter-propagating π-pulses incident on the ions to be entangled. These pulse groups are defined by fixed ratios of pulses, and some global scaling of pulse number given by the factor n. Further details of this scheme can be found in Sec. 2 of the supplemental material [38].

Ions can only be trapped in 3D by a time-averaged potential. The time-dependent potential used to generate this trapping is given by:

$$\Phi(x, y, z, t) = \frac{U}{2}(\alpha x^2 + \beta y^2 + \gamma z^2)$$
$$+ \cos(\omega_{\mathrm{RF}} t)\frac{\tilde{U}}{2}(\alpha' x^2 + \beta' y^2 + \gamma' z^2), \quad (1)$$

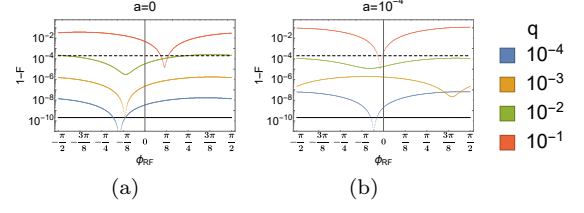which has previously been shown to lead to the following

FIG. 2. Gate that are optimised assuming an absence of micromotion typically have a decreasing fidelity under micromotion. We show fidelities for such gates plotted with respect to the phase offset between the first gate pulse and the RF drive. They are shown for a variety of values for a and q, using trap parameters $\chi = 1.8 \times 10^{-4}$, $d = 100$ μm, and $\omega = 2\pi$ MHz. Gate fidelities without micromotion indicated in solid black. Increasing values of q indicate an increasing dynamic trapping potential $\tilde{U}$, and show reduced fidelity. Here and in the figures though-out this manuscript, the black dashed line shows the fault tolerant threshold of 2×10^{-4} or equivalently a fidelity of 99.98%

approximate motion [32]:

$$x(t) \approx 2AC_0 \sin\left(\beta_x \frac{\omega_{\mathrm{RF}}}{2} t\right)\left[1 - \frac{q_x}{2}\cos(\omega_{\mathrm{RF}} t + \phi_{\mathrm{RF}})\right],$$
$$(2)$$

where A and C_0 are arbitrary constants determined by boundary conditions, and β_x, a_x, and q_x are given by

$$\beta_x \approx \sqrt{a_x + \frac{q_x^2}{2}}, a_x = \frac{4Z|e|U\alpha}{m\omega_{\mathrm{RF}}^2}, q_x = -\frac{2Z|e|\tilde{U}\alpha'}{m\omega_{\mathrm{RF}}^2}.$$

This looks like harmonic motion with a secular trapping frequency of $\omega = (1/2)\beta_x\omega_{\mathrm{RF}}$, and an additional high-frequency oscillation which is the micromotion. While this is a compact closed form approximation, designing gates with high fidelity requires a more accurate integration of the motion to a higher order. We consider gates between neighbouring ions in the x-axis of this model and set $q = q_x$. Our results are presented in units of the trapping period given by $\tau = 1/\omega$.

We use the state-averaged fidelity F as the measure of a gate's performance in this work because it can be calculated with high efficiency [31, 36, 39]. Inclusion of the micromotion adds additional terms to the analytic expression of infidelity, as detailed in the supplementary material. As we are interested in gates with fidelity close to unity, it is sensible to report this in terms of the infidelity $1 - F$. We then simplify this expression around perfect motional restoration and a $\pi/4$ phase, giving the infidelity expression as

$$1 - F \approx \frac{2}{3}\Delta\phi^2$$
$$+ \frac{4}{3}\sum_p\left(\frac{1}{2} + \overline{n}_p\right)\left((b_p^1)^2 + (b_p^2)^2\right)\Delta P_p{}^2, \quad (3)$$

where $\Delta\phi$ is the error in the phase, ΔP_p is the displacement of the pth mode in phase-space, b_p^n is the coupling of
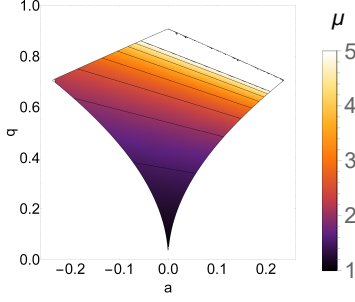
FIG. 3. The values of μ are shown as colour gradients over the stable region of trapping parameters a and q. The region to the top right of the image diverges towards infinity, but this is generally not a useful region as it results from RF frequencies close to the trapping frequencies.

the pth mode to the nth ion, and $\overline{n}_p$ is the mean motional occupation of the pth mode. We assume to be $\overline{n}_p = 0.1$ throughout this work, for larger mode occupations the infidelity will grow linearly with $\overline{n}_p$. For clarity, we include an indicative threshold for fault-tolerant quantum computing of 2×10^{-4} [40], which is indicated by a dashed black line in all relevant figures.

For the purposes of designing fast gates, traps are well characterised by the dimensionless parameter χ, given as the scaled difference between the breathing and common motional modes $\chi = \frac{\omega_{\text{BR}} - \omega}{\omega}$ in the direction of the laser-induced motion [31]. Expressions for χ in terms of trap parameters depend on the geometry, and are given in Sec. 4 of the supplementary material [38]. In the presence of micromotion, numerical integration shows that the absolute value of χ increases with a and q, which in turn leads to an increased phase acquisition rate. For radial motion in linear traps χ is negative, indicating a phase acquisition rate of the opposite sign to gates conducted using the longitudinal modes. In this case we optimise for a controlled phase gate with opposite relative phase. If needed, this could be modified to the standard controlled phase by the addition of a single qubit π-phase gate.

When optimising gate performance for the FRAG scheme, or any scheme that seeks to optimise pulse timings, the cost function becomes prohibitively complex in the presence of micromotion. To simplify this, the repetition rate can be locked to the RF-drive frequency. When this is the case, the micromotion term loses its time dependence and depends only on the phase ϕ_{RF} between the RF-drive and the laser repetition. We now introduce the parameter μ to quantify the enhancement from the effects of this scheme achieved through micromotion. We define μ as the relative increase in the maximum displacement of the ions D over the maximum displacement of the ions in a simple harmonic potential D', achieved through a momentum kick. This will be given as:
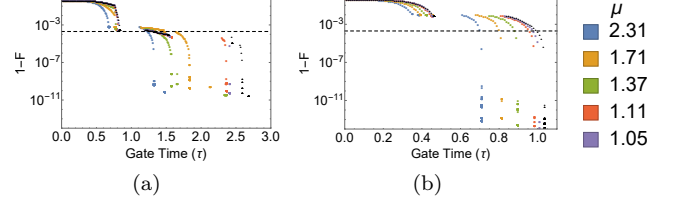

FIG. 4. Infidelities of optimised two-qubit gates with pulses occurring at π phase to RF drive, equivalent to a repetition rate locked to the trap RF drive frequency at this phase. Shown with increasing dynamic trapping potential $\tilde{U}$ indicated by increasing values of μ. (a) Microtrap architecture with $\chi = 1.8 \times 10^{-4}$ ($d = 100~\mu$m, $\omega = 2\pi$ MHz) (b) Linear Paul trap using axial modes with $\chi = -1.4 \times 10^{-2}$ ($\omega_L/\omega_A = 1/6$). The results shown as black triangles indicate the infidelities for equivalent systems without the inclusion of micromotion. This shows that both systems benefit from a clear micromotion enhancement.

$$\mu \approx \left(1 - \frac{2\left(\beta^2 + 4\right) q \cos(\phi_{\text{RF}})}{\left(\beta^2 - 4\right)^2} \right)^2$$

The infidelity expression with the inclusion of micromotion can be written as:

$$\Delta P_p = 2\mu \sqrt{\frac{\omega}{\omega_p}} \sum_k z_k \sin\left(\omega_p t_k\right), \tag{4}$$

$$\Delta \phi = \left| \sum_p 8\eta^2 \mu \frac{\omega}{\omega_p} b_p^1 b_p^2 \sum_{i \neq j} z_i z_j \sin\left(\omega_p |t_i - t_j|\right) \right| - \frac{\pi}{4}.$$

The values of the parameter μ are shown in Fig 3 for values of a and q, with the perimeter of the plot marking out the stable trapping regions within the parameter space. The full expression of μ, and its derivation are given in Sec. 5 of the supplementary material [38].

We now look at the effect micromotion has on a two-qubit gate that was optimised for a system without micromotion. We observe a decreasing fidelity as the dynamic trapping potential $\tilde{U}$ is increased, seen in Fig. 2. Taking into account the effects of finite repetition rate would significantly further reduce the fidelity. As will be shown later in this manuscript, micromotion makes fast gate schemes particularly sensitive to finite repetition rate. A successful implementation of a fast-gate using state-dependent kicks therefore requires both RF-induced micromotion and finite repetition rate to be accounted for in the optimisation process.

We now examine gates that are designed to operate in the presence of micromotion. The rate of phase acquisition will be maximised when the pulses occur at the maximum trapping point of the RF cycle, so We examine
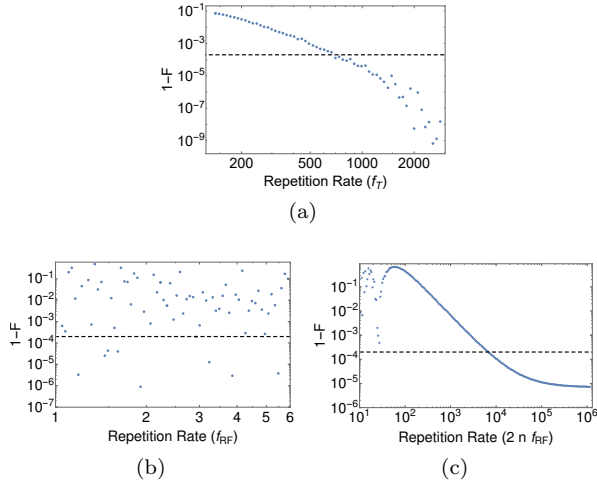
(a)

(b)

(c)

FIG. 5. Infidelity of FRAG gates taking into account finite repetition rate of the laser. We examine a case shown in Fig. 4a, where a gate in the microtrap architecture achieved infidelity of 10^{-9}, with $\mu = 2.31$ and $\chi = 1.8 \times 10^{-4}$. (a) Infidelity assuming the repetition rate is equal to the RF-drive frequency, where gate times are shifted to align with laser pulses. The repetition rate is given in terms of the secular trapping frequency f_T. (b) & (c) Infidelity of gates where the repetition rate is allowed to be higher than the RF-drive frequency. We example gates optimised for a locked repetition rate, but implemented with a finite repetition rate not locked to the RF-drive. This is shown for a repetition rate just above the RF-drive and for repetition rates greater than $2nf_{\mathrm{RF}}$.

the case where the repetition rate is locked to the RF-drive with a phase between them of $\phi_{\mathrm{RF}} = \pi$. We find that the performance of two-qubit gates improves with the amount of micromotion, with fidelity increasing with μ, which corresponds to an increased a and q. This improvement in shown in Fig. 4 for both a microtrap array (a), and the axial modes of a linear Paul trap (b). Although only one choice of gate parameter n is shown, the improvement is present for all choices of n. The plateaus in the infidelity observed for some gate times can be attributed to the anti-symmetric nature of the gate scheme, which is not favoured for gate times that are multiples of half a trapping period.

The optimised gates shown in Fig. 4 assume large instantaneous momentum kicks, whereas in practice these are composed of many small kicks. These small kicks can be made to occur simultaneously using a series of optical delay loops [41], however, this is complex and requires a high degree of accuracy on the pulse timings [31]. A simpler method is to produce pulses at a fixed repetition rate and use a pulse picker to select a subset for use in the gates. In Fig. 5a, we examine a gate that can achieve high fidelity in the limit of infinite repetition rate (one of the points Fig. 4a), and examine its fidelity assuming the repetition rate is equal to the RF drive frequency. We see that our FRAG gates are robust to this approximate implementation, with the gate achieving its maximum
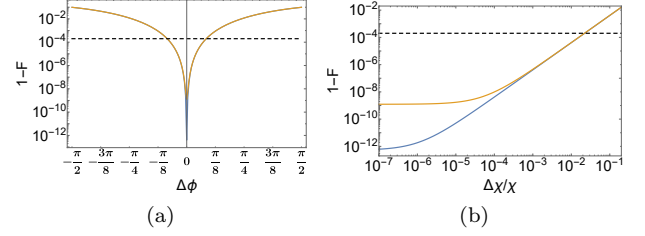

(a)

(b)

FIG. 6. Plots showing the impact to infidelity arising from realistic experimental errors for a gate with ideal infidelity 10^{-9} in microtrap architecture shown in orange ($\chi = 1.3 \times 1.8 \times 10^{-4}, \tau_G = 1.0, n = 30, \mu = 2.31$) and an axial mode gate with ideal infidelity 10^{-13} on a linear Paul trap shown in blue ($\chi = -1.3 \times 1.4 \times 10^{-2}, \tau_G = 0.7, n = 12, \mu = 2.31$) (a) Errors in the phase between laser pulses and the RF-drive. (b) Response to an error $\Delta\chi$ between the real value of χ and the value used to find an optimised gate.

fidelity in the limit of high repetition rate.

Restricting the repetition rates to be equal to the RF-drive to will in general limit the allowable repetition rate dramatically, as oscillation frequencies are generally not above 100 MHz and repetition rates of 5 GHz [42] have been demonstrated. Thus this requirement would become a limiting factor in gate time. Fortunately, if a repetition rate faster than the drive frequency is used, we find that FRAG-scheme gates can still achieve high fidelities in the presence of micromotion. In this case, the repetition rate must be carefully selected. Some repetition rates don't permit high fidelity gates due to the positioning of pulses in the RF-drive cycle. This can be seen in Fig. 5 (b) & (c). For repetition rates above $2nf_{\mathrm{RF}}$, where n is the factor described in the gate scheme, the largest pulse trains in the scheme will fit inside a single RF-cycle. To achieve high fidelity gates in this case, the repetition rate must be carefully selected or above $1000 \times 2n \times f_{\mathrm{RF}}$.

We now explore the effects of experimental errors that may be encountered using a pulse-picker to deliver the pulse trains. We begin by examining what happens when the phase between the pulses arriving and the RF-drive is not exactly π. As seen in Fig. 6 (a), gates remain below error correction infidelity thresholds until there are phase mismatches on the order of $1/16$ of an RF period. The largest RF drives encountered in most experiments are on the order of 100 MHz, equating to a requirement for nanosecond accuracy for the delay between RF drive and repetition rate.

The second form of experimental error we examine is the effect of imprecise characterisation of the trap, such as the trapping frequencies or distances between microtraps. Such errors woould lead to an incorrect estimate of χ. Fig. 6 (b) shows that gates are also robust to ssuch errors, remaining below error correction infidelity thresholds until errors of approximately 10% of the true value

of χ, corresponding with a $\sim 5\%$ error in d, or $\sim 10\%$ error in ω. In the case of the axial modes of a linear Paul trap, this corresponds to a 10% error in the ratio between the longitudinal and axial trapping frequencies.

We conclude that the micromotion present in ion trap experiments, either in microtraps or Paul traps, may be harnessed to enhance the gate times and infidelities of fast gates using ultrafast pulses. We have presented a straightforward technique to implement this enhancement by locking the RF drive and repetition rate, and have also presented the conditions under which repetition rates faster than the RF drive may be used with high fidelity. We have further shown that this method remains robust to realistic experimental error that would be encountered when implementing such fast gates. The results obtained here may be further enhanced in systems using cylindrical ring traps, as they have stable regions with a higher values of q and a [32].

---

* alex_ratcliffe@hotmail.com

[1] M. A. Nielsen and I. L. Chuang, *Cambridge University Press* (Cambridge University Press, 2010) p. 702.

[2] Y. Makhlin, G. Schön, and A. Shnirman, Nature (1999), 10.1038/18613.

[3] P. Neumann, N. Mizuochi, F. Rempp, P. Hemmer, H. Watanabe, S. Yamasaki, V. Jacques, T. Gaebel, F. Jelezko, and J. Wrachtrup, Science (New York, N.Y.) **320**, 1326 (2008).

[4] E. Knill, R. Laflamme, and G. J. Milburn, Nature (2001), 10.1038/35051009.

[5] D. G. Cory, A. F. Fahmy, and T. F. Havel, Proceedings of the National Academy of Sciences (1997), 10.1073/pnas.94.5.1634.

[6] C. Nayak, S. H. Simon, A. Stern, M. Freedman, and S. Das Sarma, Reviews of Modern Physics (2008), 10.1103/RevModPhys.80.1083.

[7] D. Loss and D. P. DiVincenzo, Physical Review A - Atomic, Molecular, and Optical Physics (1998), 10.1103/PhysRevA.57.120.

[8] B. E. Kane, Nature **393**, 133 (1998).

[9] F. Dolde, V. Bergholm, Y. Wang, I. Jakobi, B. Naydenov, S. Pezzagna, J. Meijer, F. Jelezko, P. Neumann, T. Schulte-Herbrüggen, J. Biamonte, and J. Wrachtrup, Nature Communications (2014), 10.1038/ncomms4371.

[10] M. Veldhorst, C. H. Yang, J. C. C. Hwang, W. Huang, J. P. Dehollain, J. T. Muhonen, S. Simmons, A. Laucht, F. E. Hudson, K. M. Itoh, A. Morello, and A. S. Dzurak, Nature **526**, 410 (2014).

[11] R. Barends, J. Kelly, A. Megrant, A. Veitia, D. Sank, E. Jeffrey, T. C. White, J. Mutus, A. G. Fowler, B. Campbell, Y. Chen, Z. Chen, B. Chiaro, A. Dunsworth, C. Neill, P. O'Malley, P. Roushan, A. Vainsencher, J. Wenner, A. N. Korotkov, A. N. Cle-

land, and J. M. Martinis, Nature (2014), 10.1038/nature13171.

[12] A. G. Fowler, M. Mariantoni, J. M. Martinis, and A. N. Cleland, Physical Review A - Atomic, Molecular, and Optical Physics **86** (2012), 10.1103/PhysRevA.86.032324.

[13] D. P. DiVincenzo, Fortschritte der Physik **48**, 771 (2000).

[14] G. Waldherr, Y. Wang, S. Zaiser, M. Jamali, T. Schulte-Herbrüggen, H. Abe, T. Ohshima, J. Isoya, J. F. Du, P. Neumann, and J. Wrachtrup, Nature (2014), 10.1038/nature12919.

[15] M. Veldhorst, J. C. Hwang, C. H. Yang, A. W. Leenstra, B. De Ronde, J. P. Dehollain, J. T. Muhonen, F. E. Hudson, K. M. Itoh, A. Morello, and A. S. Dzurak, Nature Nanotechnology (2014), 10.1038/nnano.2014.216.

[16] N. Friis, O. Marty, C. Maier, C. Hempel, M. Holzäpfel, P. Jurcevic, M. B. Plenio, M. Huber, C. Roos, R. Blatt, and B. Lanyon, Physical Review X **8**, 021012 (2018).

[17] C. Hempel, C. Maier, J. Romero, J. McClean, T. Monz, H. Shen, P. Jurcevic, B. P. Lanyon, P. Love, R. Babbush, A. Aspuru-Guzik, R. Blatt, and C. F. Roos, Physical Review X **8**, 31022 (2018).

[18] A. H. Myerson, D. J. Szwer, S. C. Webster, D. T. Allcock, M. J. Curtis, G. Imreh, J. A. Sherman, D. N. Stacey, A. M. Steane, and D. M. Lucas, Physical Review Letters (2008), 10.1103/PhysRevLett.100.200502.

[19] C. J. Ballance, T. P. Harty, N. M. Linke, M. A. Sepiol, and D. M. Lucas, Physical Review Letters (2016), 10.1103/PhysRevLett.117.060504.

[20] D. Nigg, M. Müller, E. A. Martinez, P. Schindler, M. Hennrich, T. Monz, M. A. Martin-Delgado, and R. Blatt, Science (2014), 10.1126/science.1253742.

[21] D. Leibfried, B. DeMarco, V. Meyer, D. Lucas, M. Barrett, J. Britton, W. M. Itano, B. Jelenković, C. Langer, T. Rosenband, and D. J. Wineland, Nature **422**, 412 (2003).

[22] J. P. Gaebler, T. R. Tan, Y. Lin, Y. Wan, R. Bowler, A. C. Keith, S. Glancy, K. Coakley, E. Knill, D. Leibfried, and D. J. Wineland, Physical Review Letters (2016), 10.1103/PhysRevLett.117.060505.

[23] J. J. Garcia-Ripoll, P. Zoller, and J. I. Cirac, Physical Review A - Atomic, Molecular, and Optical Physics **71** (2004), 10.1103/PhysRevA.71.062309.

[24] L. M. Duan, Physical Review Letters **93**, 100502 (2004).

[25] R. L. Taylor, C. D. B. Bentley, J. S. Pedernales, L. Lamata, E. Solano, A. R. R. Carvalho, and J. J. Hope, Scientific Reports **7**, 46197 (2017).

[26] C. D. B. Bentley, A. R. R. Carvalho, and J. J. Hope, New Journal of Physics **17** (2015), 10.1088/1367-2630/17/10/103025.

[27] V. M. Schäfer, C. J. Ballance, K. Thirumalai, L. J. Stephenson, T. G. Ballance, A. M. Steane, and D. M. Lucas, Nature **555**, 75 (2018).

[28] J. D. Wong-Campos, S. A. Moses, K. G. Johnson, and C. Monroe, Physical Review Letters **119**, 230501 (2017).

[29] K. G. Johnson, J. D. Wong-Campos, B. Neyenhuis, J. Mizrahi, and C. Monroe, Nature Communications **8**, 697 (2017).

[30] E. Shimshoni, G. Morigi, and S. Fishman, Physical Review Letters (2011), 10.1103/PhysRevLett.106.010401.

[31] A. K. Ratcliffe, R. L. Taylor, A. R. R. Carvalho, and J. J. Hope, Physical Review Letters **120**, 220501 (2018).

[32] D. Leibfried, R. Blatt, C. Monroe, and D. Wineland, Reviews of Modern Physics **75**, 281 (2003).

[33] D. Porras and J. I. Cirac, Physical Review Letters **96**, 250501 (2006).

[34] L. H. Nguyen, A. Kalev, M. D. Barrett, and B.-G. Englert, Physical Review A - Atomic, Molecular, and Optical Physics (2012), 10.1103/PhysRevA.85.052718.

[35] A. Bermudez, P. Schindler, T. Monz, R. Blatt, and M. Müller, New Journal of Physics (2017), 10.1088/1367-2630/aa86eb.

[36] C. D. B. Bentley, A. R. R. Carvalho, and J. J. Hope, New Journal of Physics **17** (2015), 10.1088/1367-2630/17/10/103025.

[37] J. J. Garcia-Ripoll, P. Zoller, and J. I. Cirac, Physical Review Letters **91**, 157901 (2003).

[38] "See supplemental material at end of this document.".

[39] C. D. B. Bentley, R. L. Taylor, A. R. R. Carvalho, and J. J. Hope, Physical Review A - Atomic, Molecular, and Optical Physics **93** (2016), 10.1103/PhysRevA.93.042342.

[40] J. Benhelm, G. Kirchmair, C. F. Roos, and R. Blatt, Nature Physics **4**, 463 (2008).

[41] C. D. B. Bentley, A. R. R. Carvalho, D. Kielpinski, and J. J. Hope, New Journal of Physics **15** (2013), 10.1088/1367-2630/15/4/043006.

[42] D. Heinrich, M. Guggemos, M. Guevara-Bertsch, M. I. Hussain, C. F. Roos, and R. Blatt, arXiv preprint arXiv:1812.08537 (2018).

Supplementary Material

I. TRAPPING POTENTIAL AND MICROMOTION

The model used is given as a set of individual traps (microtraps) arranged in a single line. Each microtrap is simply a Paul trap that contains only a single ion, it is thus generally not elongated along an axis as linear Paul traps are. The potential energy in this situation is then given as the sum of the trapping potentials and the Coulomb potentials between the ions:

$$V_M = \frac{e^2}{4\pi\varepsilon_0} \sum_{i=1}^{N-1} \sum_{j=i+1}^{N} \frac{1}{((j-i)d + x_j - x_i)} + \frac{1}{2}M\frac{a - 2q\cos(\omega_{RF}t)}{4}\omega_{RF}^2 \sum_{i=1}^{N} x_i^2$$

$$V_P = \frac{e^2}{4\pi\varepsilon_0} \sum_{i=1}^{N-1} \sum_{j=i+1}^{N} \frac{1}{\sqrt{(x_j - x_i)^2 + (z_j - z_i)^2}} + \frac{1}{2}\frac{M}{4}\omega_{RF}^2 \sum_{i=1}^{N} (a_z z_i^2 + (a_x - 2q_x\cos(\omega_{RF}t)x_i^2) \tag{1}$$

where x_i is the position of the ith ion in the chain relative to the centre of its own trap, d is the separation between each microtrap, ω is the angular trapping frequency of each microtrap, M is the ion mass and N the number of ions in the chain. Both of these can be approximated without micromotion as

$$V_M \approx \frac{e^2}{4\pi\varepsilon_0} \sum_{i=1}^{N-1} \sum_{j=i+1}^{N} \frac{1}{((j-i)d + x_j - x_i)} + \frac{1}{2}M\omega^2 \sum_{i=1}^{N} x_i^2$$

$$V_P \approx \frac{e^2}{4\pi\varepsilon_0} \sum_{i=1}^{N-1} \sum_{j=i+1}^{N} \frac{1}{\sqrt{(x_j - x_i)^2 + (z_j - z_i)^2}} + \frac{1}{2}M\omega^2 \sum_{i=1}^{N} (\kappa^2 z_i^2 + x_i^2) \tag{2}$$

where ω is the frequency of the approximated simple harmonic oscillator. These equations are then used to solve for the normal modes ω_p. For a single ion in a quadrapole trap the general form of the motion can be expressed as

$$x(\tau) = Ae^{i\tau} \sum_{n=-\infty}^{\infty} C_n e^{\frac{i2n(\tau + \phi_{RF})}{\beta}} + Be^{-i\tau} \sum_{n=-\infty}^{\infty} C_n e^{-\frac{i2n(\tau + \phi_{RF})}{\beta}} \tag{3}$$

As has previously been presented [1], the lowest order solutions to the resulting differential equation takes the form

$$x(t) \approx 2AC_0 \cos\left(\beta_x \frac{\omega_{RF}}{2}t\right) \left[1 - \frac{q_x}{2}\cos(\omega_{RF}t + \phi_{RF})\right]$$

Where A, C_0 are arbitrary constants determined by boundary conditions, and β_x, a_x, and q_x are given by

$$\beta_x \approx \sqrt{a_x + \frac{q_x^2}{2}}, a_x = \frac{4Z|e|U\alpha}{m\omega_{RF}^2}, q_x = -\frac{2Z|e|\tilde{U}\alpha'}{m\omega_{RF}^2}$$

For efficient simulation of the motion of ions, we use a normal mode expansion. This approximates the motion in terms of N oscillatory modes, each mode described by some frequency of oscillation ω_p and coupling to the ions $\vec{b}_p$. This is done by linearising the potential around the ions stationary points and is valid for sufficiently small displacements of the ions around their stationary points. This will then give the motion

$$x_i = A_p b_p^i e^{i\frac{\omega_p}{\omega}\tau} \sum_{n=-\infty}^{\infty} C_n e^{\frac{i2n(\tau + \phi_{RF})}{\beta}} + B_p b_p^i e^{-i\frac{\omega_p}{\omega}(\tau + \phi_{RF})} \sum_{n=-\infty}^{\infty} C_n e^{-\frac{i2n\tau}{\beta}} \tag{4}$$

with the amplitudes of each mode A_p, B_p and the phase of each mode ϕ_p determined by initial conditions. The frequency of the approximated simple harmonic oscillator will be given in terms of β and ω_{RF} as $\omega = \frac{1}{2}\beta\omega_{\text{RF}}$. With the presence of micromotion these modes will have shifted frequencies, these shifts can be found by numerical integration or a continued fraction [2]. To appropriately match the phase evolution of the ODE the first order solution is not sufficient, and we need to take the Fourier expansion in Eq.4 to the 5th term.

II.   GATE SCHEME

We analyse fast gate schemes that use a series of broadband counter-propagating π-pulses, incident on the two ions to which the gate is to be applied. These π-pulses can be simple square pulses of the appropriate height, or shaped for convenience of production or robustness of the change of state. They are always used in counter-propagating pairs so that they do not change the internal state of the ions, but give them a state-dependent momentum kick. These kicks are significant due to the Lamb-Dicke parameter, which is typically of the order of $\eta \approx 0.16$. These state-dependent kicks then have a state-dependent effect on the energy (and phase evolution) of those modes through interaction via the Coulomb potential. Correctly chosen kicks can ultimately return the motional state of the ions to their initial state, leaving the net effect of a controlled phase gate:

$$\hat{U}_{\text{CPhase}} = e^{i\frac{\pi}{4}\sigma_1^z \sigma_2^z} \tag{5}$$

A general fast gate can be described by a set of pulse timings $\vec{t}$ and pulse-group intensities $\vec{z}$. Different pulse-group intensities are generated by having different numbers of single pulses comprising a pulse-group. These single pulses then arrive at, or symmetrically around, the pulse time given for that group, hence the pulse intensities are given as integer multiples. Multiple fast gate schemes have been proposed in the literature, such as: GZC [3], Duan [4] and FRAG [5]. Each scheme imposes a different set of restrictions on the number of distinct pulses, symmetry and different ratios of pulse numbers in pulse groups. For the FRAG scheme, the timings of theses pulses and the number of pulses in each pulse group are given by the vectors $\underline{t}$ and $\underline{z}$ respectively:

$$\underline{t} = (-\tau_1, -\tau_2, -\tau_3, \tau_3, \tau_2, \tau_1),$$
$$\underline{z} = (-n, 2n, -2n, 2n, -2n, n). \tag{6}$$

The sign of the components of $\underline{z}$ corresponds to changing the direction of the initially incident pulse, and the factor of n is an integer that characterises the overall scale of numbers of pulses at each time. With an infinite repetition rate laser, To produce an effective C-Phase gate the timings (τ_1, τ_2, τ_3) are chosen to give the desired gate. In the original FRAG scheme proposal there was a strict ordering on the magnitude of (τ_1, τ_2, τ_3). In this implementation we do not impose a strict ordering of the times (τ_1, τ_2, τ_3), effectively resulting in a set of six possible pulse schemes. The total gate time is therefore twice the maximum of the values of τ_1, τ_2, and τ_3.
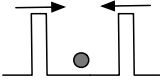
a) Train of pulse pairs
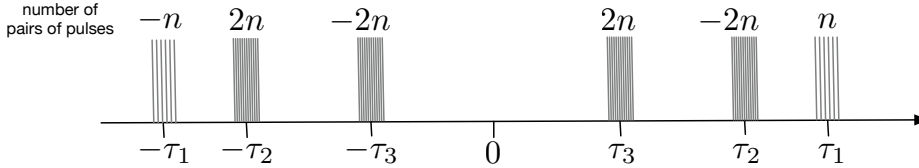
b)   Pulse pair

FIG. 1. a) Diagram with the pulse timing for the FRAG scheme. The components z_j of the z vector indicate the number of pairs of pulses that hit the ion at each time τ_j. The sign in z_j indicates which pulse within each pair (shown in b) reaches the ion first. This gives the sign of the momentum kick imprinted on the ion.

III. FIDELITY CALCULATIONS IN THE ABSENCE OF MICROMOTION

We use numerical searches to find pulse timings that produce high quality gate operations, with the state-averaged fidelity F, given as the integral of the square of the norm of the overlap between the post-gate state with the target state integrated over all initial states. This is efficient to compute and it is strongly related to other distance measures for high-fidelity gates. As we examine fidelities extremely close to unity, we report the infidelity $1 - F$. This is a function of the phase mismatch $\Delta\phi$ around the target $\pi/4$ phase, and the phase space displacement of the motional modes ΔP_p given without micromotion as

$$\Delta P_p = 2\sqrt{\frac{\omega}{\omega_p}} \sum_k z_k \sin\left(\omega_p t_k\right)$$

$$\Delta\phi = \left| \sum_p 8\eta^2 \frac{\omega}{\omega_p} b_p^1 b_p^2 \sum_{i\neq j} z_i z_j \sin\left(\omega_p |t_i - t_j|\right) \right| - \frac{\pi}{4} \tag{7}$$

For efficient computation of two-ion gates, we further simplify this measure by using a truncated expansion of the infidelity in these variables:

$$1 - F \approx \frac{2}{3}\Delta\phi^2 + \frac{4}{3}\sum_p (\frac{1}{2} + \tilde{n}_p)((b_p^1)^2 + (b_p^2)^2)\Delta P_p{}^2 \tag{8}$$

where $\tilde{n}_p$ is the mean motional occupation of the pth mode. While this approximate form is efficient for generating gate schemes, we use the full form when reporting achievable fidelities, for example, in the presence of multiple ions. We can see from Eq. (8) that the infidelity for a two-ion system, $1 - F$, depends on the Lamb-Dicke parameter η, the angular frequencies collective motional modes ω_n, the coupling of the k-th ion to the p-th mode, b_p^k, and the number of pulses in the i-th pulse train z_i. The collective mode frequencies ω_n can be calculated from the mass of the ions M, the separation of the microtraps d, and the trapping frequency ω of the individual microtraps.

We search for pulse timings that produce optimal gate fidelity within a given time bound. This optimisation is run as a set of local gradient searches in the three-dimensional parameter space of the pulse timings, over a large set of initial gate sequences. The highest fidelity of these local optimisations is then taken to be the optimal gate for that cap in the gate time. Note that the optimal gate occasionally takes less time than the maximum allowed. By increasing the cap in total gate time and repeating this process, we map out the optimal fidelity for fast gates as a function of gate time.

IV. KEY PARAMETER FOR CHARACTERISING TRAPS

We see from Eq. 8 that the system behaviour depends on the ratios of the frequencies of the collective modes. These are in turn functions of the geometry, and the dimensionless parameter $\xi = \frac{d^3\omega^2}{\alpha}$, where $\alpha = \frac{e^2}{4\pi\varepsilon_0}\frac{1}{M}$. Here e is the electron charge, M the mass of the ions, and ε_0 the vacuum permittivity.

For a two-ion system, there is only one ratio, so it entirely characterises the behaviour. We define χ as the normalised difference between the breathing mode frequency and the common motional mode frequency $\chi = \frac{\omega_{\text{BR}} - \omega}{\omega}$ which can be expressed in terms of the more fundamental parameter ξ as following:

$$\chi = \sqrt{\frac{1}{3}\left(9 - \beta\gamma^{\frac{1}{3}} + \beta\gamma^{\frac{2}{3}}\right)} - 1 \tag{9}$$

where

$$\gamma = 1 + \frac{3(9 + \sqrt{3}\sqrt{27 + 2\xi})}{\xi}$$

and

$$\beta = 9 - \sqrt{3}\sqrt{27 + 2\xi}$$